Calculating transport of water from a conduit to the porous matrix by Boundary Distributed Source Method

Matija Perne[a], Božidar Šarler[b], Franci Gabrovšek[a]

[a] *Karst Research Institute ZRC SAZU, Titov trg 2, SI-6230 Postojna, Slovenia*
[b] *University of Nova Gorica, Laboratory for Multiphase Processes, Vipavska 13, SI-5001 Nova Gorica, Slovenia*

Abstract

The objective of the study is application of a new boundary meshless numerical method to geohydrological problems. An application of the non-singular version of the method of fundamental solutions (MFS) to moving boundary (Stefan) problems arising in Darcy flow from a conduit to isotropic and homogeneous porous matrix is described. The motivation for the study represents assessment of a suitable numerical method for porous media flow with free and moving boundaries. The solution in two-dimensional Cartesian coordinates is represented in terms of the fundamental solution of the Laplace equation. The desingularisation of the diagonal terms is achieved through boundary distributed sources of fundamental solution and indirect calculation of the derivatives of fundamental solution. Respectively, the artificial boundary, characteristic for the classical, singular MFS, does not need to be present. This is advantageous, particularly in the treated free and moving boundary problems, since only the geometry of the physical boundary needs to be manipulated. Several numerical examples, exhibiting a moving boundary between the wetted and non-wetted porous media are shown. The novel method is compared with the classical method of fundamental solutions and analytical solutions with excellent agreement. A sensitivity study of model parameters is performed.

The new contribution of the study is application of the BDS method to free and moving boundary problems and comparison of BDS with MFS for such type of problems.

Keywords: karst aquifer, Darcy flow, Stefan problem, moving and free boundary problems, method of fundamental solutions, boundary distributed source method

1. Introduction

The exchange of flow and solutes between the conduits and the surrounding matrix plays an important role in many engineering and geohydrological problems [1]. A related example are karst aquifers, where the conduits are usually embedded into a fractured-porous medium. There, the storage and the transport of potential pollutants through the aquifer depends on the exchange processes between the potentially polluted conduits and the matrix [2, 3]. It is therefore of importance to understand the dynamics of these exchange processes and to consider them in realistic models of karst aquifer.

The analytical solutions of such models can be obtained only for a very limited, geometrically simple, linear two-dimensional cases [4, 5].

Different coupled continuum pipe-flow models have been used in the past to numerically model flow and solute transport in karst aquifers. These models rely on finite difference method (FDM) [6, 7] or finite element method (FEM) [8, 9] discretisation scheme. They have successfully captured the dynamics of flow and transport in cou-

Email addresses: matija.perne@zrc-sazu.si (Matija Perne), bozidar.sarler@ung.si (Božidar Šarler), gabrovsek@zrc-sazu.si (Franci Gabrovšek)

pled conduit-matrix systems. One has to consider the presence of a water table, a moving (transient character) boundary or free (steady character) boundary between the saturated and the unsaturated zone in the case of unconfined aquifers.

In cases when the mesh based methods, such as the FDM or FEM, are used for solving the above mentioned problems, various mesh refinement schemes are invoked to numerically account for a suitable determination of the position of the unfixed boundary. The principal bottleneck in these types of numerical methods is the time consuming re-meshing of the evolving water table and wetted/unwetted domains which limits such methods to problems with quite trivial geometrical patterns [10].

In order to build effective models for such situations, computationally new and efficient, meshfree modelling concepts [11, 12, 13, 14], have to be considered.

Meshfree methods have proven to be very efficient in treating complex moving boundaries [15]. This work presents the use of such methods for a computational model of a conduit embedded in a matrix. It is focused on studying the exchange between a conduit and unconfined matrix due to a sudden change of pressure in the conduit. The Method of Fundamental Solutions (MFS) and its non-singular version, termed the Boundary Distributed Source method (BDS) proposed by Liu in [16], are used to model a related moving boundary problem. Our objectives are in demonstrating the use of BDS in problems related to groundwater flow, achieving advantages over classical numerical methods, and studying its sensitivity to model parameters.

MFS is a numerical technique that falls in the class of methods generally called boundary methods. The other well known representative of these methods is the Boundary Element Method (BEM). Both methods are best applicable in situations where a fundamental solution to the partial differential equation under consideration is known. In such cases, the dimensionality of the discretisation is reduced. BEM for example requires polygonisation of the boundary surfaces in general 3D cases, and boundary curves in general 2D cases. This method requires solution of the complicated regular, weakly singular, strongly singular, and hypersingular integrals over boundary segments, which is usually a cumbersome and non-trivial task [17].

Both, BEM [18, 19] and MFS [15, 20], are well suited for unfixed boundary (Stefan) problems [21] due to the fact that only the boundary discretisation needs to be moved, without any connection with the domain discretisation.

A comprehensive survey of the MFS and related methods for elliptic boundary value problems and inverse problems can be found in [22, 23]. The MFS has certain advantages over BEM, that are mostly visible in the fact that pointisation of the boundary is needed only, that completely avoids any integral evaluations, and makes no principal difference in coding between the 2D and the 3D cases. The principal drawback of MFS is the presence of artificial boundary which needs to be constructed in cases with the singular fundamental solution (such as for example the fundamental solution of the Laplace equation) in order to allow the solution to comply with the boundary conditions. The MFS with the artificial boundary has been previously used in the context of transport of pollutants in porous media [24] and in the context of free surface flow [25].

The determination of the distance between the real boundary and the fictitious boundary is based on experience, by balancing between the increased accuracy and the increased ill-conditioning with the larger distance. Quite recently, various efforts have been made to remove this drawback of the MFS, so that the source points can be placed on the real boundary directly. Young et al. [26] were the first to propose placing of the source points on the boundary in the MFS. They proposed novel ways to directly determine the diagonal coefficients for simple geometries or use the results from the BEM, based on the fact that the MFS and the indirect boundary integral formulation are similar in nature. In their approach, the information of the neighbouring points before and after each source point is needed in order to form the line segments for integrating the kernels to obtain the diagonal coefficients in general. This is essentially the same information of the element connectivity

as in a BEM mesh. Šarler [27] proposed a similar modified MFS, where the diagonal terms are determined by the integration of the singular or hypersingular fundamental solution on line segments, formed by using neighbouring points, and the use of a constant solution to determine the diagonal coefficients from the derivatives of the related fundamental solution. This first attempts have been followed by the formulation [16], where in order to remove the singularities of the fundamental solutions, the concentrated point sources are replaced by the distributed sources over areas (for 2D problems) or volumes (for 3D problems) covering the source points. The distributed sources, associated with the derivatives of the fundamental solution, have been however calculated as in [27]. Liu called his non-singular MFS approach BDS. It is the purpose of the present paper to solve the moving boundary problem, associated with the conduit and the porous matrix by the BDS and compare it with the classical MFS and analytical solutions.

2. Governing equations

Throughout the paper we consider the porous matrix to be homogeneous and isotropic, we neglect the capillary and evaporation effects, we consider 2D situation, the flow follows Darcy law [28, 29, 30, 31, 32, 33], hydraulic conductivity or permeability of the fractured rock is constant and isotropic. The liquid-saturated part of the matrix is represented by a connected two-dimensional domain Ω with boundary Γ. The medium is described by its hydraulic conductivity $\tilde{K}$ and porosity Φ. The problem is tackled in Cartesian coordinates $\tilde{\mathbf{p}} = \tilde{x}\mathbf{i_x} + \tilde{y}\mathbf{i_y}$, where $\tilde{x}$ and $\tilde{y}$ represent the Cartesian coordinates and $\mathbf{i_x}$ and $\mathbf{i_y}$ the base vectors. The gravity is directed toward $-\mathbf{i_y}$.

The quasi steady state fluid flow in Ω is described by Darcy law

$$\tilde{\mathbf{q}} = -\tilde{K}\tilde{\nabla}\tilde{h}, \tag{1}$$

where $\tilde{\mathbf{q}}$ is flux and $\tilde{h}$ the hydraulic head. A length scale l_0 is selected. Dimensionless coordinates are defined as $x = \tilde{x}/l_0$ and $y = \tilde{y}/l_0$, $\mathbf{p} = \tilde{\mathbf{p}}/l_0$. Dimensionless flux $\mathbf{q} = \tilde{K}^{-1}\tilde{\mathbf{q}}$ with $h = \tilde{h}/l_0$ are introduced in order that $\nabla = l_0\tilde{\nabla}$. Eq. 1 can afterwards be rewritten in dimensionless form

$$\mathbf{q} = -\nabla h. \tag{2}$$

Incompressibility is assumed and thus the specific storage in comparison with the specific yield is neglected. Incompressibility implies

$$\nabla \cdot \mathbf{q} = 0 \tag{3}$$

in the whole domain Ω. Eqs. 2 and 3 give Laplace equation for the dimensionless hydraulic head in Ω

$$\nabla^2 h = 0. \tag{4}$$

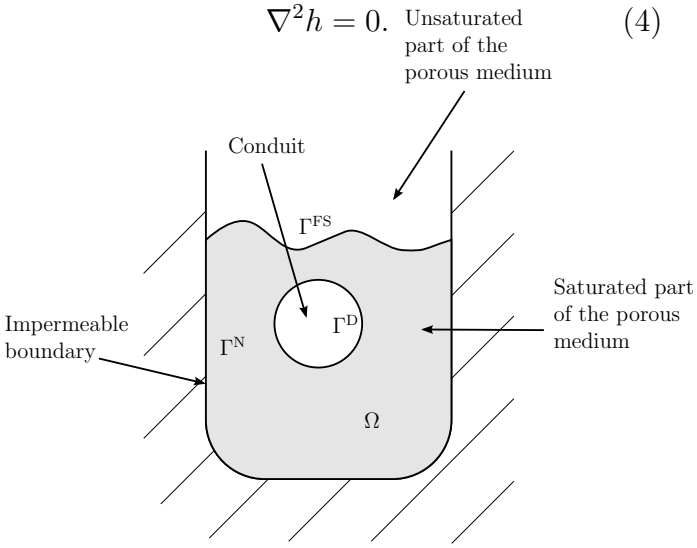

Figure 1: Schematics of the problem domain and the boundary conditions.

The boundary is divided into three parts with Dirichlet, Neumann and free surface boundary conditions; i.e. $\Gamma = \Gamma^{\mathrm{D}} \cup \Gamma^{\mathrm{N}} \cup \Gamma^{\mathrm{FS}}$ (see Fig. 1). On Γ^{D} there is a Dirichlet type of boundary condition. The hydraulic head is specified with the forcing function h^{D},

$$h\left(\mathbf{p}\right) = h^{\mathrm{D}}\left(\mathbf{p}\right), \quad \mathbf{p} \in \Gamma^{\mathrm{D}}. \tag{5}$$

On Γ^{N} there is a Neumann type of boundary condition. The hydraulic head gradient is specified with the forcing function q^{N}

$$\frac{\partial h}{\partial \mathbf{n}_{\Gamma}^{\mathrm{N}}}\left(\mathbf{p}\right) = q^{\mathrm{N}}\left(\mathbf{p}\right), \quad \mathbf{p} \in \Gamma^{\mathrm{N}}, \tag{6}$$

where $\mathbf{n}_{\Gamma}^{\mathrm{N}}$ is the outward normal to the boundary Γ^{N} and $q^{\mathrm{N}}\left(\mathbf{p}\right)$ is the normal component of

flow. For the Laplace equation, the liquid surface Γ^{FS} represents a special case of Dirichlet boundary condition. The free surface boundary condition is defined through the height

$$h\left(\mathbf{p}\right) = y\left(\mathbf{p}\right), \quad \mathbf{p} \in \Gamma^{\mathrm{FS}}. \tag{7}$$

The liquid surface represents a moving boundary. The velocity of a point at the moving boundary is

$$\frac{\partial \mathbf{p}}{\partial t} = -\nabla h\left(\mathbf{p}\right), \quad \mathbf{p} \in \Gamma^{\mathrm{FS}}, \tag{8}$$

where t is dimensionless time, $t = \tilde{t}\tilde{K}/(\phi l_0)$, and $\tilde{t}$ is time. Eq. 8 can be projected onto the normal to the surface $\mathbf{n}_\Gamma^{\mathrm{FS}} = n_x\mathbf{i}_\mathbf{x} + n_y\mathbf{i}_\mathbf{y}$

$$\mathbf{n}_\Gamma^{\mathrm{FS}} \cdot \frac{\partial \mathbf{p}}{\partial t} = \mathbf{n}_\Gamma^{\mathrm{FS}} \cdot \big(-\nabla h\left(\mathbf{p}\right) \big). \tag{9}$$

The free surface is almost horizontal in all the calculated cases so n_x is much smaller to n_y and is neglected. The free surface is thus moved in every timestep according to equation

$$\frac{\partial y}{\partial t} = -\frac{\partial h}{\partial y}. \tag{10}$$

It is the purpose of the present work to calculate the hydraulic head (4) and the time evolution of the boundary Γ^{FS} as a function of the boundary conditions (5–10) and initial position of Γ^{FS}.

3. Solution procedure

3.1. Solution of Laplace equation

3.1.1. Method of fundamental solutions

The MFS is based on the basic theory of partial differential equations (PDEs), stating that any linear combination of the solutions of a linear PDE is also a solution. The method belongs to the class of boundary meshless methods for solving various types of partial differential equations and started to be increasingly applied in engineering since 1964 [34].

The solution is built as a linear combination of fundamental solutions of Laplace equation $G_i(\mathbf{p})$. By definition of a fundamental solution, G_i solves the equation

$$\nabla^2 G_i = \delta\left(\mathbf{p}_i\right), \tag{11}$$

where $\nabla^2 = \frac{\partial^2}{\partial x^2} + \frac{\partial^2}{\partial y^2}$ and $\delta\left(\mathbf{p}\right)$ is Dirac delta function. Fundamental solution is also a solution of Laplace equation (Eq. 4) outside $\mathbf{p}_i$. Its form is [16]

$$G_i(\mathbf{p}) = -\frac{1}{2\pi}\log\left(\|\mathbf{p} - \mathbf{p}_i\|\right),$$

$$\|\mathbf{p} - \mathbf{p}_i\| = \sqrt{(\mathbf{p} - \mathbf{p}_i)\cdot(\mathbf{p} - \mathbf{p}_i)}. \tag{12}$$

The solution is built as the sum

$$h\left(\mathbf{p}\right) \approx \sum_{\mathrm{i}=1}^{N} G_{\mathrm{i}}\left(\mathbf{p}\right) c_{\mathrm{i}}, \tag{13}$$

where N is the number of all fundamental solutions and c_{i} are the coefficients. Note that the positions of the singularities $\mathbf{p}_{\mathrm{i}}$ have to be outside $\Omega + \Gamma$ so that h solves Laplace equation inside $\Omega + \Gamma$. The line that connects the singularities is called artificial boundary (Fig. 2). The coefficients are determined by collocating the boundary conditions. Each point with Dirichlet boundary condition gives an equation

$$\sum_{\mathrm{i}=1}^{N} G_{\mathrm{ij}} c_{\mathrm{i}} = h_{\mathrm{j}},$$

$$G_{\mathrm{ij}} = G_{\mathrm{i}}(\mathbf{p}_{\mathrm{j}}), \quad h_{\mathrm{j}} = h^{\mathrm{D}}(\mathbf{p}_{\mathrm{j}}), \quad \mathbf{p}_{\mathrm{j}} \in \Gamma^{\mathrm{D}}. \tag{14}$$

In case of Neumann boundary conditions, the row

$$\sum_{\mathrm{i}=1}^{N} K_{\mathrm{ij}} c_{\mathrm{i}} = q_{\mathrm{j}},$$

$$K_{\mathrm{ij}} = \frac{\partial G_{\mathrm{i}}}{\partial \mathbf{n}}\left(\mathbf{p}_{\mathrm{j}}\right) = -\frac{1}{2\pi}\frac{(\mathbf{p}_{\mathrm{j}} - \mathbf{p}_{\mathrm{i}})\cdot\mathbf{n}}{\|\mathbf{p}_{\mathrm{j}} - \mathbf{p}_{\mathrm{i}}\|^2},$$

$$q_{\mathrm{j}} = q^{\mathrm{N}}\left(\mathbf{p}_{\mathrm{j}}\right), \quad \mathbf{p}_{\mathrm{j}} \in \Gamma^{\mathrm{N}} \tag{15}$$

follows from every boundary point. Both sets of equations are solved together as one matrix equation. A square system of linear equations is assembled from the rows (14) and (15) for solution of N unknown coefficients c_{i}.

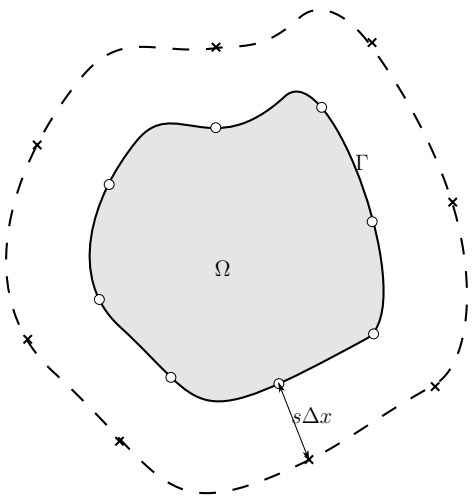

Figure 2: Concept of MFS. Small white circles are collocation nodes with specified boundary condition, crosses are the fundamental solution singularities, and the dashed line is artificial boundary $s\Delta x$ away from geometrical boundary.

3.1.2. Boundary distributed source method

BDS method is conceptually similar to MFS and the principal difference between both methods is in choice of the basis functions [16]. In MFS, the fundamental solutions are used as basis functions, while in BDS, the solutions for distributed area sources are used. The chosen shape of the source is a circle A of a radius r_0 with uniform source density of $1/(\pi r_0^2)$. The form of the solution is equal to the integral of the original fundamental solution G on A [16]

$$\hat{G}_\mathrm{i}(\mathbf{p}) = \begin{cases} \frac{r_0^2}{2}\log\left(\frac{1}{\|\mathbf{p}-\mathbf{p}_\mathrm{i}\|}\right) & \text{for } \|\mathbf{p}-\mathbf{p}_\mathrm{i}\| > r_0; \\ \frac{r_0^2}{2}\log\left(\frac{1}{r_0}\right) + \frac{r_0^2 - \|\mathbf{p}-\mathbf{p}_\mathrm{i}\|^2}{4} & \text{for } \|\mathbf{p}-\mathbf{p}_\mathrm{i}\| \leq r_0. \end{cases} \tag{16}$$

As the basis functions have no singularities, they can be centred on the boundary points, thus no separate choice of the source points $\mathbf{p}_\mathrm{i}$ is needed (Fig. 3). The solution of Laplace equation is approximated as

$$h(\mathbf{p}) \approx \sum_{\mathrm{i}=1}^{N} \hat{G}_\mathrm{i}(\mathbf{p})\, c_\mathrm{i}, \tag{17}$$

where N is the number of all boundary points and c_i are the coefficients. The coefficients are determined from the boundary conditions. Each point with Dirichlet boundary condition gives an equation

$$\sum_{\mathrm{i}=1}^{N} \hat{G}_\mathrm{ij} c_\mathrm{i} = h_\mathrm{j},$$

$$\hat{G}_\mathrm{ij} = \hat{G}_\mathrm{i}(\mathbf{p}_\mathrm{j}), \quad h_\mathrm{j} = h^\mathrm{D}(\mathbf{p}_\mathrm{j}), \quad \mathbf{p}_\mathrm{j} \in \Gamma^\mathrm{D}. \tag{18}$$

The equation that follows from each boundary point in the case of Neumann boundary conditions is

$$\sum_{\mathrm{i}=1}^{N} \hat{K}_\mathrm{ij} c_\mathrm{i} = q_\mathrm{j}, \quad q_\mathrm{j} = q^\mathrm{N}(\mathbf{p}_\mathrm{j}), \quad \mathbf{p}_\mathrm{j} \in \Gamma^\mathrm{N}. \tag{19}$$

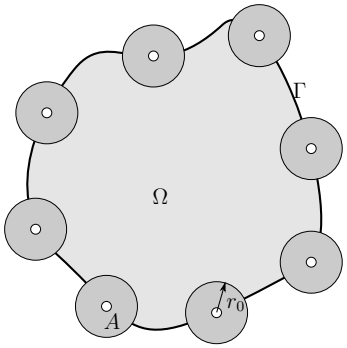

Figure 3: Concept of BDS. Small white circles are collocation nodes with specified boundary condition, dark grey circles A are distributed sources with radius r_0.

Typically $\hat{K}_\mathrm{ij}$ is taken to be the normal component of the gradient of $\hat{G}_\mathrm{i}$: $\hat{K}_\mathrm{ij} = \partial \hat{G}_\mathrm{i}(\mathbf{p}_\mathrm{j}) / \partial \mathbf{n}(\mathbf{p}_\mathrm{j})$. By this definition, the diagonal terms of the matrix, corresponding to the collocation points with Neumann boundary conditions, would always equal zero. However, an indirect method is used instead of it [27]. First, Dirichlet boundary condition $h(\mathbf{p}_\mathrm{j}) = 1$ is used for all the boundary points in Γ and coefficients c_i^c are obtained. As the normal component of gradient is presumably zero in the case of the solution for a constant value, the diagonal terms can be expressed as

$$\hat{K}_\mathrm{ii} = -\frac{1}{c_\mathrm{i}^\mathrm{c}} \sum_{\substack{\mathrm{j}=1 \\ \mathrm{j}\neq\mathrm{i}}}^{N} \hat{K}_\mathrm{ij} c_\mathrm{j}^\mathrm{c}. \tag{20}$$

Both sets of equations are solved together as one matrix equation. A square system of linear equations is assembled from the rows (18) and (19) for solution of N unknown coefficients c_i.

3.2. Free parameters of the methods

In MFS, the free parameter of the method represents the distance of the artificial boundary from the geometrical boundary. In BDS, the free parameter of the method represents the radius of the desingularisation circle.

3.3. Symmetry

Consider a situation where the geometry and the fields exhibit reflection symmetry. Let us distribute the sources of the basis functions consistently with this symmetry. Respectively, for every basis function, there is another one centred on its mirror image. In the solution sum, both basis functions are multiplied by the same coefficient. The sum of such a symmetric couple of basis functions is effectively treated as a single basis function.

All the cases considered in the present paper exhibit the reflection symmetry. The coordinate system is always positioned so that the axis of symmetry lies at $x = 0$. When a basis function is centred on $(x_\mathrm{i}, y_\mathrm{i})$ its mirror image is centred on $(-x_\mathrm{i}, y_\mathrm{i})$. The calculations are performed only for $x \geq 0$, on $x < 0$ half-plane no boundary points have to be prescribed.

3.4. Treatment of moving boundary

To calculate the displacement of the moving boundary, the head gradient is needed according to Eq. 10. The equation for the head gradient has the same form as the equation given by the Neumann boundary condition. In the case of MFS, its y component is

$$\frac{\partial h}{\partial y}\left(\mathbf{p}_\mathrm{j}\right) = \sum_{\mathrm{i}=1}^{N} \frac{\partial G_\mathrm{i}}{\partial y}\left(\mathbf{p}_\mathrm{j}\right) c_\mathrm{i}, \tag{21}$$

and in the case of BDS

$$\frac{\partial h}{\partial y}\left(\mathbf{p}_\mathrm{j}\right) = \sum_{\mathrm{i}=1}^{N} F_\mathrm{ij} c_\mathrm{i}. \tag{22}$$

Here,

$$F_\mathrm{ij} = \frac{\partial \hat{G}_\mathrm{i}}{\partial y}\left(\mathbf{p}_\mathrm{j}\right), \quad i \neq j \tag{23}$$

and

$$F_\mathrm{ii} = -\frac{1}{c_\mathrm{i}^\mathrm{c}} \sum_{\substack{\mathrm{j}=1 \\ \mathrm{j}\neq\mathrm{i}}}^{N} F_\mathrm{ij} c_\mathrm{j}^\mathrm{c} \tag{24}$$

The boundary points are moved together with the boundary, as follows from Eq. 10 and Euler backward formula

$$y_\mathrm{j}^\mathrm{new} = y_\mathrm{j} - \frac{\partial h}{\partial y}\left(\mathbf{p}_\mathrm{j}\right) \Delta t. \tag{25}$$

$y_\mathrm{j}^\mathrm{new}$ represents the coordinate of the boundary point in the next timestep. The derivative $\partial h/\partial y\left(\mathbf{p}_\mathrm{j}\right)$ is calculated by Eq. 21 or 22. In MFS, the artificial boundary and the singularities are moved by the same amount, while in BDS the basis functions remain centred on the moved boundary points.

3.5. Overview of the solution procedure

The flowchart of the solution procedure is presented schematically in Fig. 4. First, the geometry and the boundary conditions are defined. Then they are discretised – represented by the coordinates of the boundary points, the boundary conditions for all the boundary points and, in the case of MFS, the coordinates of the singularities of the basis functions, or in the case of BDS, the radii of the desingularisation circles.

The Laplace equation Eq. 4 is solved next, by using MFS or BDS.

From the solution of Laplace equation, the head derivative $\partial h/\partial y$ at the liquid surface is determined according to Eq. 21 in case of MFS or Eq. 22 in case of BDS. The displacement of the surface in a timestep Δt is calculated according to Eq. 25. The new shape of the liquid surface (and in the case of MFS of the artificial boundary) is determined. In particular, the new positions of the boundary points, the new boundary conditions at the boundary points and in the case of MFS the new positions of the singularities at the end of the timestep are calculated. They are used as discretised geometry and boundary conditions for the next timestep. At the same time,

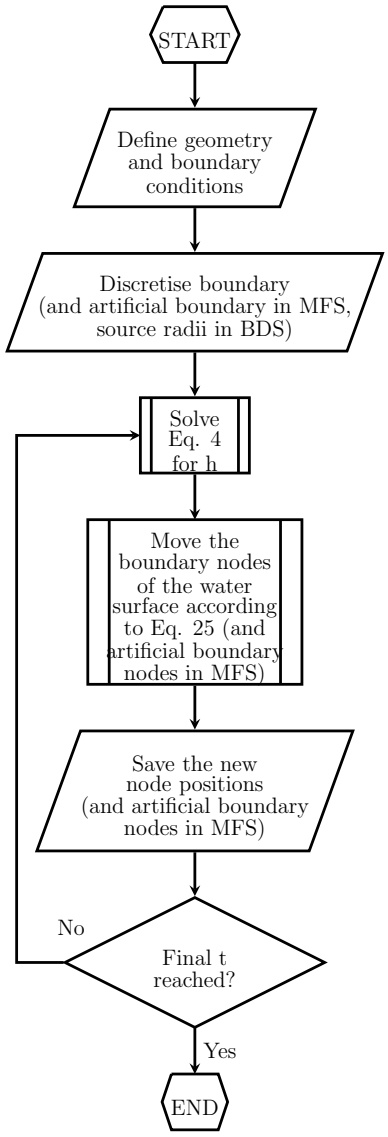

Figure 4: Flowchart of the solution procedure.

the total amount of liquid that enters the matrix is calculated from the displacement of the boundary points.

4. Numerical examples

To test the methods, two cases for which analytical results exist, were selected. In Case 1, a steady state inflow into an underground tunnel is calculated. In Case 2, a simple one dimensional problem of matrix-infilling due to a pressure change at lower boundary is calculated. The numerical results for both cases are compared with the analytical results. In Case 3, a transient exchange between the conduit and the matrix in two dimensional domain is calculated by MFS and BDS. Since this case is a main motivation for the study, several examples with different parameters are calculated.

The numerical procedures are written in C++ language and compiled with g++ 4.5.2 compiler. The matrix equations are solved using LU method implemented in Meschach++ library by Stephen Roberts. The OS used is Ubuntu 11.04 with Linux kernel 2.6.38-11-generic, 2.0 GiB of RAM and Intel® Core™2 Duo CPU E8400 with 3.00 GHz clock cycle. A calculation of a typical MFS example with $N = 200$ and 1500 steps takes approximately 10 s of CPU time.

4.1. Case 1: steady state inflow into a tunnel

Steady state inflow into an underground tunnel is investigated. The geometry of the problem and some parameters are presented in Fig. 5. R is the radius of the tunnel, H is the distance between its center and the water level surface. The water surface is flat and horizontal. The density of the boundary points and, in the case of MFS, of the singularities of the basis functions, is constant along all the straight boundaries. Δx is the distance between the boundary points. The distance between the geometrical and the artificial boundary in the case of MFS is expressed as $s\Delta x$ (Fig. 2). X is the distance between the symmetry axis and the outer edge of the domain, and Y between the water level and the lower edge.

The first boundary point at the bottom is on the symmetry axis $x = 0$, then a new one follows every Δx in $+x$ direction until $x < X$. The boundary condition on all these points is no flow, Neumann type, $\partial h/\partial y = 0$. For every boundary point there is a singularity in MFS that is at the same x and $-s\Delta x$ away from it in y direction.

There is no boundary point at the outside lower corner, the points along $x < X$ start one Δx above the bottom, the next one is one Δx in $+y$ direction until the water surface is reached. The boundary condition is again no flow, $\partial h/\partial x = 0$. For every boundary point there is a singularity in MFS that is at the same y and $s\Delta x$ away from it in x direction.

On the water surface, the points start at $x = X$ and follow until $x = 0$ at the distance Δx. The boundary condition is of Dirichlet type, $h = y$. For every boundary point there is a singularity in MFS that is at the same x and $s\Delta x$ away from it in y direction.

The points on the conduit wall are distributed uniformly along the semicircle of radius R, the first and the last ones are at both cross-sections with $x = 0$. The singularities in MFS are distributed the same way on a semicircle around the same center, only with radius $R/2$. The boundary condition is of Dirichlet type, $h = y$.

The analytical solution for the case is obtained by standard methods and is given in classical textbooks [5, 35] on groundwater hydrology. The inflow per unit length of tunnel is

$$q' = \frac{2\pi K H}{\log\left(2H/R\right)}, \tag{26}$$

where K is the hydraulic conductivity, R is the radius of the tunnel, and H is the depth of the centerline of the tunnel below the steady water table [35]. Expressed with dimensionless variables, the inflow is

$$q' = -2l_0 K \frac{\partial V}{\partial t}, \tag{27}$$

where the numerical factor 2 comes from bilateral symmetry (there is another half of space in addition to the modelled half). Both equations together give

$$-\frac{\partial V}{\partial t} = \frac{\pi H/l_0}{\log\left(2H/R\right)}. \tag{28}$$

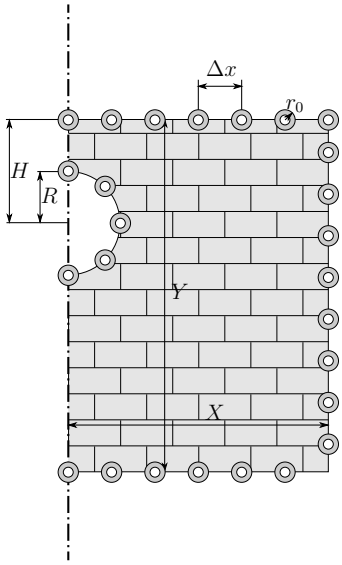

Figure 5: Case 1: Scheme of the numerical approach for BDS. Empty circles are points with the specified boundary condition, dark grey circles are the distributed sources, and the dot-dashed line is the symmetry axis.

Both MFS and BDS are applied to test the agreement with the analytical solution. The left hand side of Eq. 28 is calculated numerically and is found out to be equal to 5.888 using MFS and to 6.165 using BDS. The parameters of the calculation used are $X = 100, Y = 97, R = 1, H = 4, N = 181, \Delta x = 2$, in MFS $s = 5$, in BDS $r_0 = \Delta x/4$. There are 32 points in the conduit. The parameters on the right hand side in this geometry are $H/l_0 = 4$ and $R/l_0 = 1$ so the right hand side evaluates to 6.043. The agreement of our result with the textbook is thus very good.

4.2. Case 2: one-dimensional time-dependent case

A one-dimensional time-dependent case with a fixed head boundary condition on the lower end, a free surface boundary condition on the upper end, and gravity pointing downwards, depicted in Fig. 6, is investigated. In one-dimensional Darcy flow in homogeneous medium, the gradient of h is independent of y. If the boundary condition at

the lower boundary $y = 0$ is $h = H$, its relation to water depth P is

$$\frac{\mathrm{d}h}{\mathrm{d}y} = \frac{H - P}{P}. \tag{29}$$

By Darcy law,

$$\frac{\mathrm{d}P}{\mathrm{d}t} = \frac{\mathrm{d}h}{\mathrm{d}y}. \tag{30}$$

By eliminating the gradient of h from the equations, and integrating, we get

$$t = P_0 - P - H\Big[\ln(H - P) - \ln(H - P_0)\Big], \tag{31}$$

where $P_0 = P(t = 0)$.

The case is solved numerically using BDS. The discretised geometry, presented in Fig. 7, is similar to Case 1, only without a conduit, and the node at $x = X$ on the water surface is left out.

The boundary conditions at the bottom boundary points are of Dirichlet type, $h = H$. For the outward boundary, the boundary condition is no flow, the same as in Case 1. The upper boundary is a free surface. The boundary condition for the Laplace equation is of Dirichlet type, $h = y$, where y is the vertical coordinate of the boundary point at the particular instant.

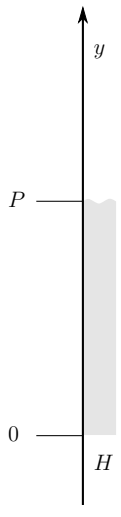

Figure 6: Case 2: The geometry of the one-dimensional time-dependent test case.

The parameters used are $X = 101$, $Y = 10$, $\Delta x = 1, \Delta t = 0.1, r_0 = \Delta x/4$, the calculation is run until $t = 100$. The bottom boundary is located at $y = 0$, the boundary condition is Dirichlet with $h = 20$. The outward boundary extends from $y = 0$ to $y = 20$. That is, the boundary points are positioned at every Δx in y direction until $y = 20$ even if they are above the initial water table. The y coordinate of the central point is used as P in Eq. 31 with $P_0 = 10$ and $H = 20$ and $t(P)$ is calculated. The difference between the numerically obtained t and $t(P)$ from Eq. 31 is presented in Fig. 8. The methods are compared in this way because Eq. 31 offers an explicit form for $t(P)$ and not for $P(t)$. The duration of the calculation is sufficient to approach the equilibrium, the change of P during the calculation is 99.6 % of the way toward $P = H$. It can be seen that the agreement is good.

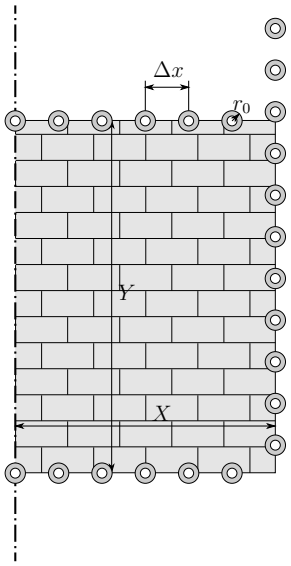

Figure 7: Case 2: Scheme of the numerical approach for BDS. Empty circles are points with the specified boundary condition, dark grey circles are the distributed sources, and the dot-dashed line is the symmetry axis. Note that some of the nodes at $x = X$ are initially located above the water table.

4.3. Case 3: Conduit-matrix exchange

The geometry of the problem and some parameters are presented in Fig. 9. R is the radius of the conduit, H is the distance between its center and the water level surface at the beginning. Initially, the water surface is flat and horizontal. The density of the boundary points and, in the

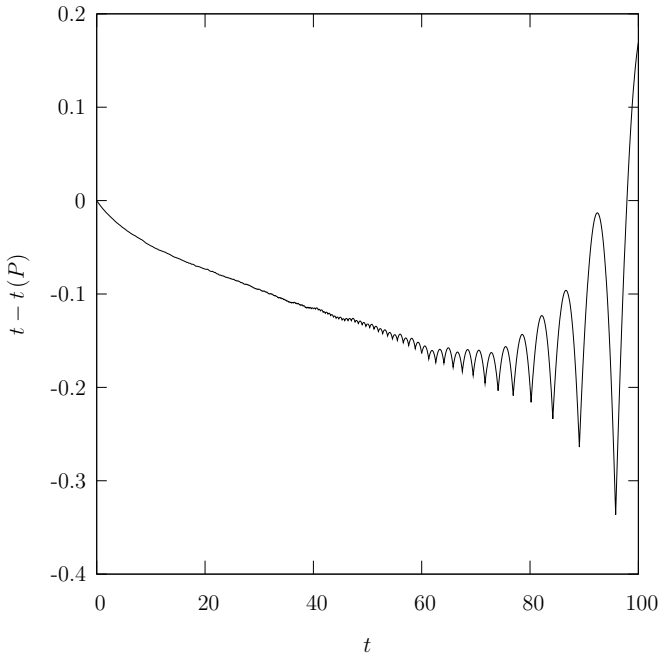

Figure 8: Case 2: Difference between t of the BDS calculation and $t\,(P)$ calculated from the BDS result for P using Eq. 31. The difference stays below 1% of t in the whole calculation.

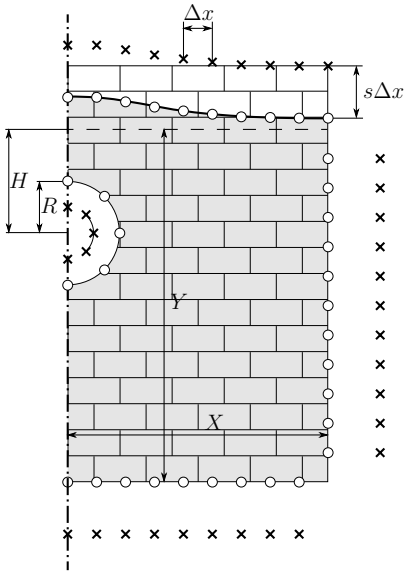

Figure 9: Case 3: Scheme of the numerical approach for MFS. Circles are points with the specified boundary condition, crosses are poles of basis functions lying on the artificial boundary, and the dot-dashed line is the symmetry axis.

case of MFS, of the singularities of the basis functions, is constant along all the straight boundaries. Δx is the distance between the boundary points. The distance between the geometrical and the artificial boundary is fixed during time. The ratio between this distance and Δx is labelled s. X is the distance between the symmetry axis and the outer edge of the domain, and Y between the initial water level and the lower edge.

Discretisation is exactly the same as in Case 1. The boundary conditions at the bottom and at the outer edge are the same as in Case 1, too. At the water surface, the free surface boundary condition is used. The boundary condition for the Laplace equation is of Dirichlet type, $h = y$, where y is the vertical coordinate of the boundary point at the particular instant. In MFS, the singularities above the free surface keep constant x and move in y direction to keep the distance from their boundary points equal to $s\Delta x$. The boundary condition at the conduit wall is of Dirichlet type, $h = H + \Delta h$.

An example of the MFS solution of the Laplace equation is presented in Fig. 10. The parameters of this example are $X = 100, Y = 97, R = 1, H = 4, \Delta h = 2, t = 150, N = 181, \Delta x = 2, s = 5, \Delta t = 0.1$. As already defined, t is dimensionless time, Δt dimensionless timestep, and N the number of all basis functions. Note that due to the nature of Laplace equation there is no initial condition, its role is taken by the initial geometry and boundary conditions. The example is calculated with 32 boundary points in the conduit so that s in the conduit is approximately the same as along the straight edges. This example is taken as the MFS standard example. The resulting hydraulic head is quite uniform around the boundaries far from the conduit, while near the conduit it rises to the prescribed $h = -1$.

An example where all the parameters are the same as for Fig. 10 but is calculated using BDS with $r_0 = \Delta x/4$ is presented in Fig. 11. It is taken as the BDS standard example. As the gradient of h is low in some areas, comparison of equipotential lines is a sensitive method for checking the similarity of potentials calculated with different methods. It can be seen that some equipotential

lines are noticeably different even if the potentials are quite similar.

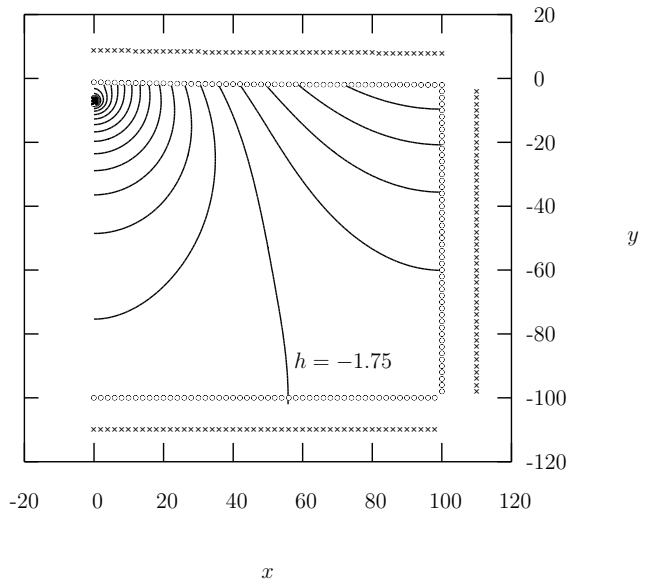

Figure 10: Case 3: Potential h at $t = 150$, calculated using MFS. The other parameters are $X = 100, Y = 97, R = 1, H = 4, \Delta h = 2, N = 181, \Delta x = 2, s = 5, \Delta t = 0.1$. The lines represent constant h and are spaced 0.05 apart. The boundary points are denoted by circles and the crosses mark the poles of the fundamental solutions.

Fig. 12 represents temporal evolution of the water table. Note that the graph is cropped in Y direction so that only the interesting part is seen. All the parameters except for t are the same as in the standard example (see Fig. 10).

The area between the original water table and the water table at time t was calculated and labelled V. It represents the volume of water that left the conduit under the assumptions of Darcy flow. The result for $V(t)$ for the standard example is presented in Fig. 13. Note that in the limit $t \to \infty$, the volume approaches $\Delta h X$, as expected.

4.3.1. Sensitivity analysis

Behaviour of MFS and BDS in calculating Case 3 is investigated. MFS is checked first, as it is the

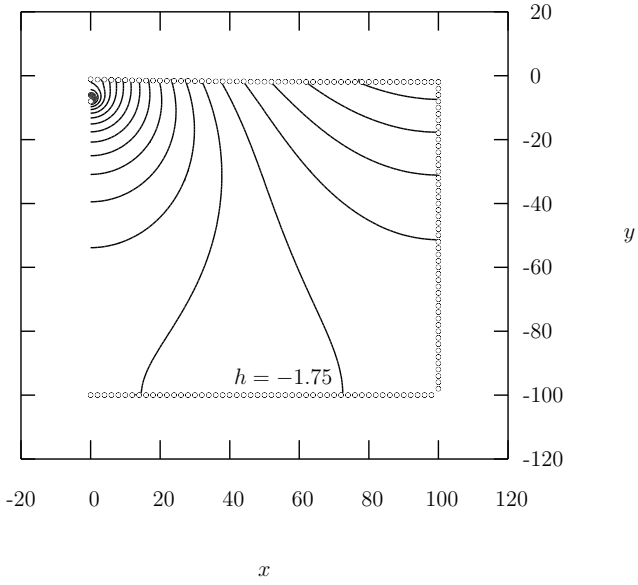

Figure 11: Case 3: Potential h at $t = 150$, calculated using BDS. The other parameters are $X = 100, Y = 97, R = 1, H = 4, \Delta h = 2, N = 181, \Delta x = 2, \Delta t = 0.1, r_0 = \Delta x/4$. The lines represent constant h and are spaced 0.05 apart. The boundary points are denoted by circles.

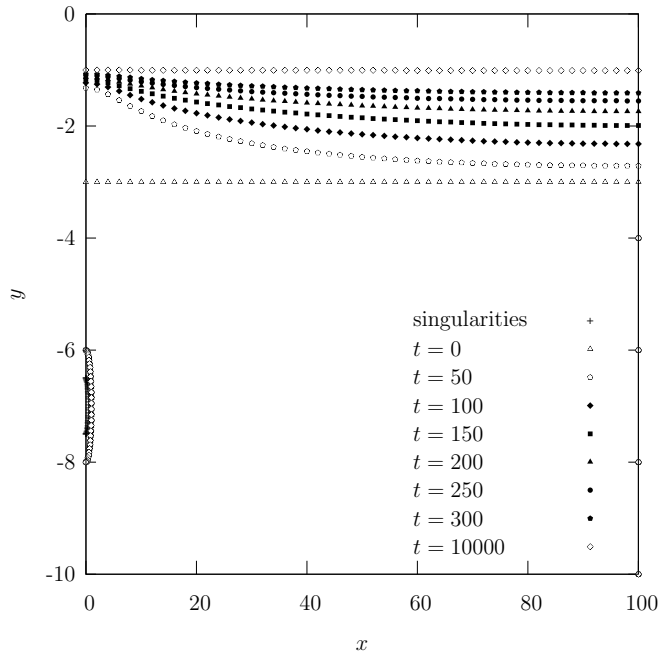

Figure 12: Case 3: The shape of Ω at different t calculated using MFS. Ω is delimited by boundary points, the singularities are outside Ω and fall outside the graph except in the conduit along the left edge (the circular conduit is not circular in the figure due to different x and y scaling). The parameters are $X = 100, Y = 97, R = 1, H = 4, \Delta h = 2, N = 181, \Delta x = 2, s = 5, \Delta t = 0.1$.

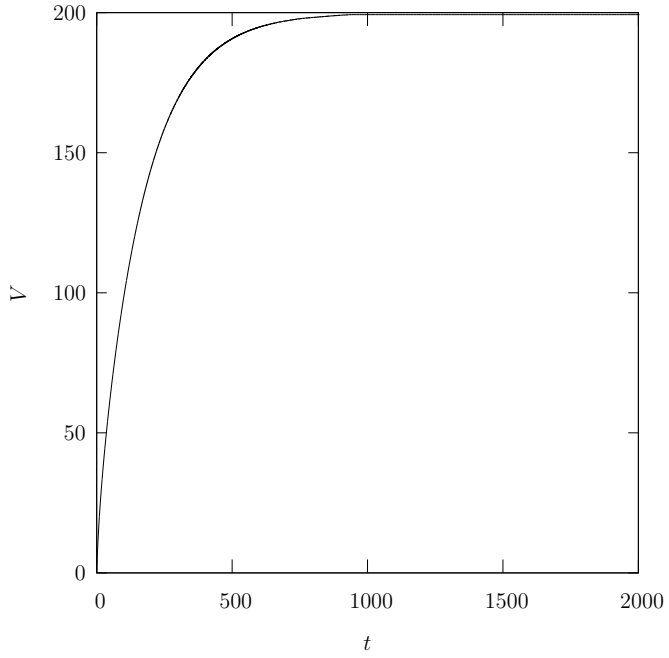

Figure 13: Case 3: Volume as a function of time, calculated until equilibrium, using BDS. The parameters are $X = 100, Y = 97, R = 1, H = 4, \Delta h = 2, N = 181, \Delta x = 2, \Delta t = 0.1, r_0 = \Delta x/4$.

more established of the two methods. BDS results are then compared to MFS results. A thorough sensitivity study of BDS is performed afterwards.

The correct result depends only on physical parameters $(X, Y, R, H, \Delta h)$ so the numerical result should not strongly depend on the chosen internal parameters of MFS $(N, \Delta x, s, \Delta t)$. In Fig. 14, the results for different values of s near $s = 5$ are presented. It can be seen that influence of s is small in the range considered.

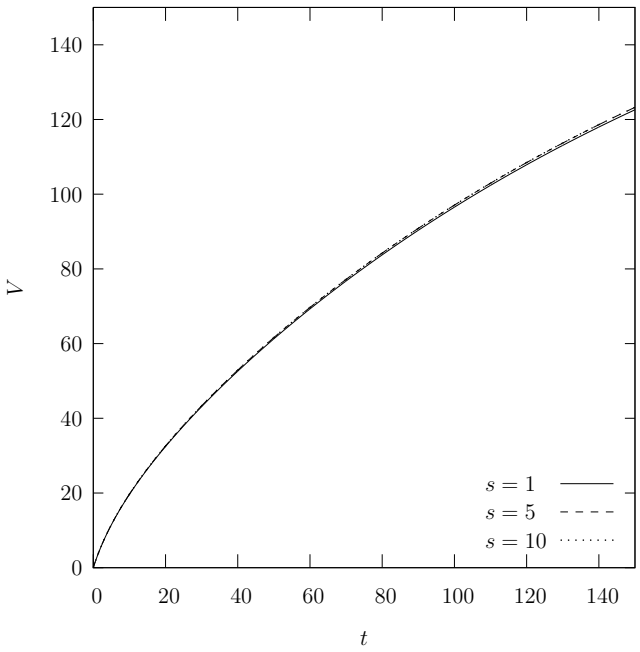

Figure 14: Case 3: Volume as a function of time, calculated for different s in MFS. The other parameters are $X = 100, Y = 97, R = 1, H = 4, \Delta h = 2, t = 150, N = 181, \Delta x = 2, \Delta t = 0.1$ as in the standard example.

The distribution and the number of boundary points is also varied. The result for the standard example, $X = 100, Y = 97, R = 1, H = 4, \Delta h = 2, t = 150, N = 181, \Delta x = 2, s = 5, \Delta t = 0.1$, is $V = 123.253$. If the number of points in the conduit is reduced to 3 so that Δx in the conduit is comparable to the one at the straight edges, the result is very similar, $V = 123.013$. Here, $N = 152$, while the other parameters stay the same. On the other hand, if the conduit is left with 32 points and Δx is enlarged to 4, then $N = 107$ and $V = 123.173$.

If the timestep is enlarged to $\Delta t = 1$ and the

other parameters are left the same as in the standard example, the result is $V = 123.497$.

In Fig. 15, the standard example is calculated by both MFS and BDS. In Fig. 16, the same is done for twice as big density of points along the straight edges. The agreement between MFS and BDS is better in the later case.

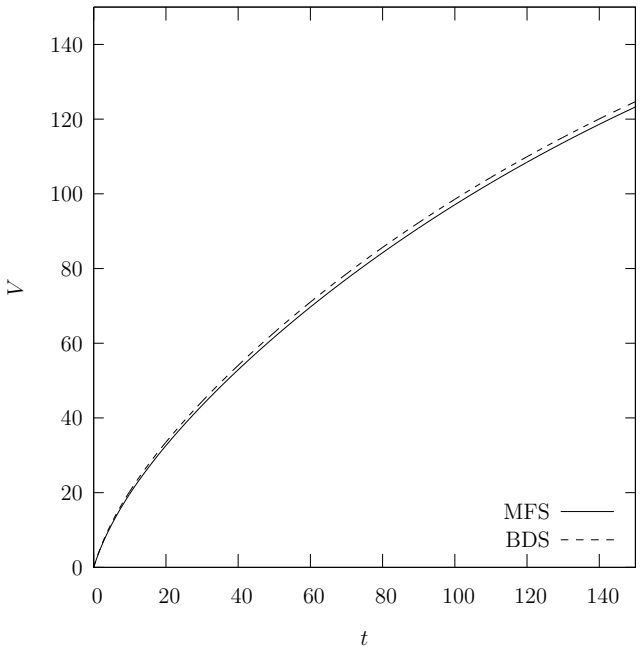

Figure 15: Case 3: Volume as a function of time, comparison between MFS and BDS. The parameters are $X = 100, Y = 97, R = 1, H = 4, \Delta h = 2, t = 150, N = 181, \Delta x = 2, s = 5, r_0 = \Delta x/4, \Delta t = 0.1$.

Sensitivity of BDS with respect to timestep Δt, source radius r_0, and the distance between the boundary points Δx is analysed. The results for sensitivity regarding Δt are presented in Fig. 17. Calculated V at $t = 150$ is more or less independent of the choice of Δt until above a critical value of Δt when it no longer converges to the correct value.

The sensitivity to $r_0/\Delta x$ is presented in Fig. 18. The sensitivity to Δx is shown in Fig. 19. For the cases with $\Delta x \geq 2$, the number of boundary points in the conduit is 3 as the circular conduit shape cannot be resolved well enough with too few points. For smaller Δx, the number of nodes in the conduit is increased so that the distance between them is similar to Δx. In the conduit, there are 5 nodes for $\Delta x = 1$, 8 nodes for $\Delta x = 0.5$,

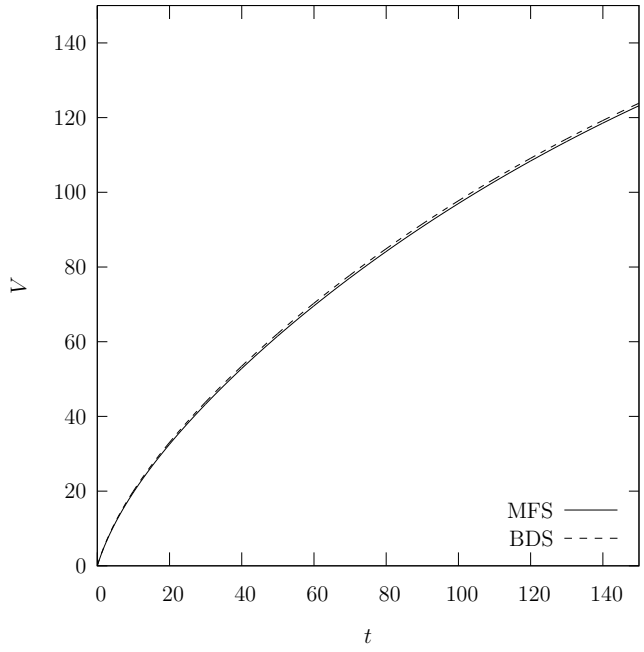

Figure 16: Case 3: Volume as a function of time, comparison between MFS and BDS. The density of the boundary points is larger than in Fig. 15, the parameters are $X = 100, Y = 97, R = 1, H = 4, \Delta h = 2, t = 150, N = 329, \Delta x = 1, s = 5, r_0 = \Delta x/4, \Delta t = 0.1$.

and 14 nodes for $\Delta x = 0.25$. The analysis for $\Delta x > 8$, where the calculated V is expected to be very different, was not performed. In these cases, the distance between the conduit and the liquid surface would fall below 1/3 of the distance between the nodes, while the nodes in the conduit part would be less than $\Delta x/5$ apart.

We see that the results, when solving the Laplace equation by MFS, do not depend strongly on s, Δx or Δt. The results obtained by BDS in place of MFS are also not significantly different. At the same time, BDS is not sensitive to Δt, r_0 or Δx in the range considered.

4.4. Discussion

BDS [16] is applied in the present paper to solve the moving/free boundary problems associated with the transport of water from the conduit to the porous matrix. The method essentially gives the same results as the classical MFS. It has the advantage that the artificial boundary is not present. This advantage is particularly welcome in the treated unfixed boundary problems, since

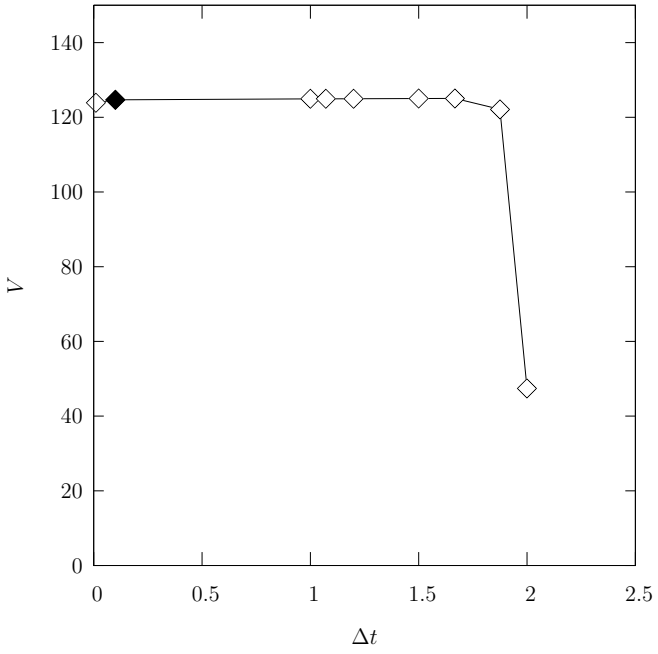

Figure 17: Case 3: Influence of the timestep on the BDS method. The other parameters are $X = 100, Y = 97, R = 1, H = 4, \Delta h = 2, t = 150, N = 181, \Delta x = 2, r_0 = \Delta x/4$. It can be seen that the results are fairly consistent up to $\Delta t = 1.875$ while at $\Delta t = 2$ the result is obviously incorrect. The full diamond corresponds to the standard example.

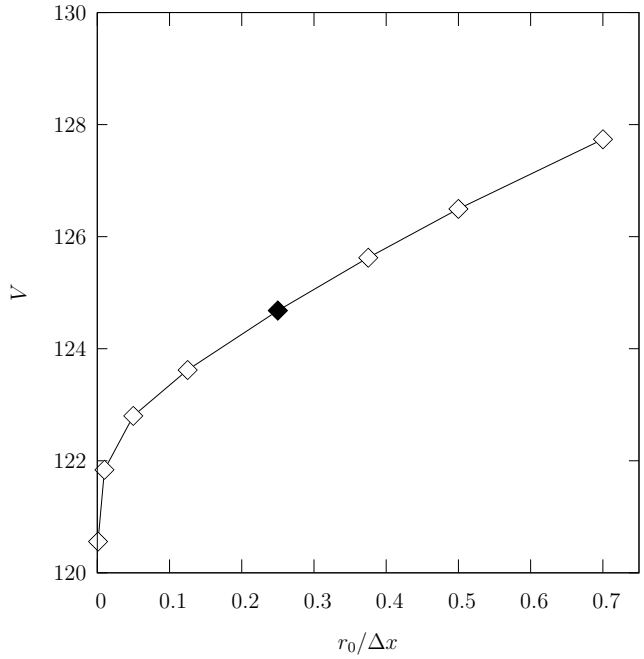

Figure 18: Case 3: Influence of the source radius r_0 on the BDS method. The other parameters are $X = 100, Y = 97, R = 1, H = 4, \Delta h = 2, t = 150, N = 181, \Delta x = 2, \Delta t = 0.1$. When r_0 changes for a factor of 700, the change in the result is a few percent. The full diamond corresponds to the standard example.

the artificial boundary does not need to be recalculated along with the physical boundary, as in the classical MFS. In BDS, only the points on the unfixed physical boundary are moved.

MFS and BDS are used to calculate water exchange between a conduit and the surrounding matrix, which is a situation, important in karst hydrogeology.

We consider a water filled conduit that is initially in equilibrium with the surrounding matrix. A step change in hydraulic head is applied and time dependent exchange flow is calculated. The results obtained by MFS and BDS are compared to each other. Sensitivity analyses of the influence of density of points, distance between the real and the artificial boundary in MFS, source radii in BDS, and timestep are done. MFS is benchmarked against a textbook solution, and BDS against a time-dependent example with analytical solution. The textbook solution is for steady state inflow into an underground tunnel. The only difference between our conduit and the tunnel is

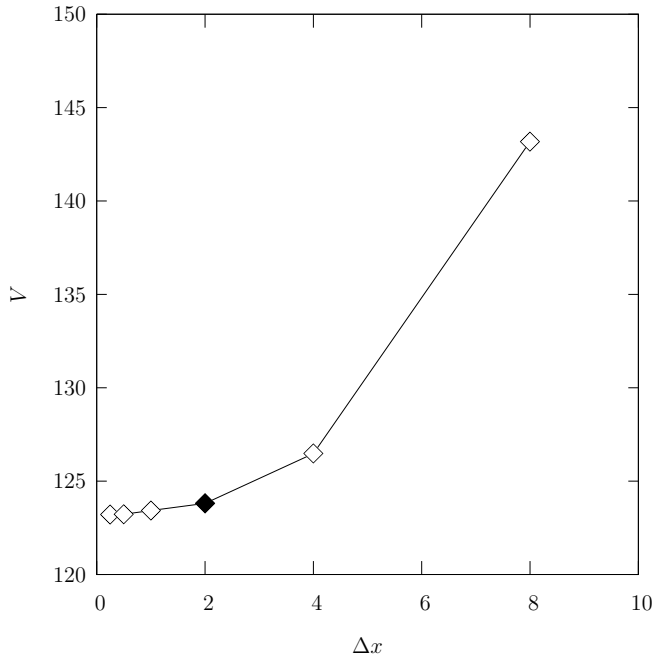

Figure 19: Case 3: Influence of the boundary point spacing Δx on the BDS method. The other parameters are $X = 100, Y = 97, R = 1, H = 4, \Delta h = 2, t = 150, r_0 = \Delta x/4, \Delta t = 0.1$. The number of boundary points varies from $N = 41$ for $\Delta x = 8$ to $N = 1202$ for $\Delta x = 0.25$. The result is changing slowly as a function of Δx and is steady for $\Delta x \to 0$. The full diamond corresponds to Δx of the standard example.

the boundary condition on the tunnel wall, where seepage face $h = y$ is used. The time-dependent analytical example is one-dimensional, oriented along gravity with fixed head boundary condition on the lower end and free surface on the upper end. It is compared to a modelled 2D rectangle with fixed head boundary condition at the lower and free surface at the upper face, no flow boundary condition at the sideways face and a symmetry axis just like the conduit-matrix exchange examples. The agreement with the benchmarks and between different runs is excellent in all the cases.

5. Conclusion

Both MFS and BDS are found to be efficient and reliable when applied to computation of moving boundary/free surface Darcy flow problems. Water exchange between a conduit and the surrounding matrix is dealt with successfully. The BDS method is applied to free and moving boundary problems for the first time and compared with MFS and analytical solutions for such type of problems. A new boundary meshless numerical method is applied to geohydrological problems and found to be suitable for the purpose.

It should be noted that in BDS the governing equation is not satisfied in the parts of the domain overlapping with the circles [16]. The method can potentially be applied to multiply-connected-domain problems [36] while it is not certain if any modifications would be needed [16]. However, the problem tackled here is essentially simply-connected due to the consideration of the symmetry.

The BDS method presented in this paper is very general and it can be adapted or extended to handle many related problems, discussed in the present paper. We will address the anisotropic and the three dimensional situations in our future publications. We are also searching for the possibility to calculate the diagonal coefficients for the Neumann boundary condition in a direct way.

6. Acknowledgement

This work was funded by the Slovenian Research Agency (ARRS) in the framework of basic

research project J2-4093: Development and application of advanced numerical methods in study of karst processes, and research programmes P2-0379 and P6-0119.

References

[1] Nield D, Bejan A. Convection in porous media. Berlin: Springer; third edition ed.; 2006.

[2] Ford DC, Williams PW. Karst hydrogeology and geomorphology. John Wiley & Sons; 2007.

[3] Hu BX. Examining a coupled continuum pipe-flow model for groundwater flow and solute transport in a karst aquifer. Acta carsologica 2010;39(2):347 –59.

[4] Leontiev A, Huacasi W. Mathematical programming approach for unconfined seepage flow problem. Engineering Analysis with Boundary Elements 2001;25:49–56.

[5] Raghavan R, Ozkan E. A Method for Computing Unsteady Flows in Porous Media; vol. 318 of *Pitman Research Notes in Mathematics Series*. Harlow: Longman Scientific and Technical; 1992.

[6] Aitchison J. Numerical treatment of a singularity in a free boundary problem. Proceedings of the Royal Society of London Series A 1972;330:573–80.

[7] Barenblatt GE, Zheltov IP, Kochina IN. Basic concepts in the theory of seepage of homogeneous liquids in fissured rocks. Journal of Applied Mathematics and Mechanics 1960;24:1286–303.

[8] Lacy SJ, Prevost JH. Flow through porous media: a procedure for locating the free surface. International Journal for Numerical and Analytical Methods in Geomechanics 1987;11:585–601.

[9] Istok J. Groundwater Modeling by the Finite Element Method. Water resources monograph; Washington, DC: American Geophysical Union; 1989.

[10] Šarler B. Towards a mesh-free computation of transport phenomena. Engineering Analysis with Boundary Elements 2002;26:731–8.

[11] Fasshauer GF. Meshfree Approximation Methods with MATLAB. River Edge, NJ, USA: World Scientific Publishing Co., Inc.; 2007.

[12] Šarler B. From global to local radial basis function collocation method for transport phenomena. Computational Methods in Applied Sciences 2007;5:257–82.

[13] Atluri S, Shen S. The meshless local Petrov-Galerkin (MLPG) method. Contemporary research on emerging sciences and technology; Tech Science Press; 2002.

[14] Liu GR. Mesh Free Methods: Moving Beyond the Finite Element Method. Boca Raton: CRC Press; 2002.

[15] Šarler B. Solution of a two-dimensional bubble shape in potential flow by the method of fundamental solutions. Engineering Analysis with Boundary Elements 2006;30:227–35.

[16] Liu Y. A new boundary meshfree method with distributed sources. Engineering Analysis with Boundary Elements 2010;34(11):914 –9.

[17] Chen J, Hsiao C, Lee Y. Study of free-surface seepage problem using hypersingular equations. Communications in Numerical Methods in Engineering 2007;23:755–69.

[18] Queen D, Oxley M, Vosika D. The boundary element method applied to moving boundary problems. Mathematical and Computer Modelling 1990;14:145–50.

[19] Ahmed SG, Meshrif SA. A new numerical algorithm for 2d moving boundary problems using a boundary element method. Computers & Mathematics with Applications 2009;58:1302–8.

[20] Chantasiriwan S, Johansson B, Lesnic D. The method of fundamental solutions for free surface stefan problems. Eng Anal Bound Elem 2009;33:529–38.

[21] Šarler B. Stefan's work on solid-liquid phase changes. Engineering Analysis with Boundary Elements 1995;16:83–92.

[22] Fairweather G, Karageorghis A. The method of fundamental solutions for elliptic boundary value problems. Adv Comput Math 1998;:69–95.

[23] Karageorghis A, Lesnic D, Marin L. A survey of applications of the MFS to inverse problems. Inverse Problems in Science and Engineering 2011;19:309–36.

[24] Guevara-Jordan J, Rojas S. A method of fundamental solutions for modeling of porous media advective fluid flow. Applied Numerical Mathematics 2003;47:449–65.

[25] Chaiyo K, Rattanadecho P, Chantasiriwan S. The method of fundamental solutions for solving free boundary saturated seepage problem. International Communications in Heat and Mass Transfer 2011;38:249–54.

[26] Young DL, Chen KH, Lee CW. Novel meshless method for solving the potential problems with arbitrary domain. Journal of Computational Physics 2005;209:290–321.

[27] Šarler B. Solution of potential flow problems by the modified method of fundamental solutions: formulations with the single layer and the double layer fundamental solutions. Engineering Analysis with Boundary Elements 2009;33:1374–82.

[28] Darcy H. Les Fontaines Publiques de la Ville de Dijon. Paris: Victor Dalmont; 1856.

[29] Kaviany M. Principles of heat transfer in porous media. New York: Springer-Verlag; 1995.

[30] Lee C, Farmer I. Fluid flow in discontinuous rocks. London, New York: Chapman & Hall; 1993.

[31] Bear J. Dynamics of fluids in porous media. Dover books on physics and chemistry; Dover; 1988.

[32] Sahimi M. Flow and Transport in Porous Media and Fractured Rock. Weinheim: VCH Verlagsgesellschaft; 1995.

[33] Šarler B, Perko J, Gobin D, Goyeau B, Power H.

Dual reciprocity boundary element method solution of natural convection in darcy – brinkman porous media. Engineering Analysis with Boundary Elements 2004;28:23 – 41.

[34] Kupradze VD, Aleksidze MA. The method of functional equations for the approximate solution of certain boundary value problems. USSR Computational Mathematics and Mathematical Physics 1964;4:82–126.

[35] Domenico P, Schwartz F. Physical and chemical hydrogeology. Wiley; 1990.

[36] Chen K, Kao J, Chen J, Young D, Lu M. Regularized meshless method for multiply-connected-domain laplace problems. Engineering Analysis with Boundary Elements 2006;30(10):882 –96.